Experimental and calculated N(^{4}S) temporal density profile in the N_2 flowing post-discharge

2005 J. Phys. D: Appl. Phys. 38 2204

(http://iopscience.iop.org/0022-3727/38/13/019)

INSTITUTE OF PHYSICS PUBLISHING JOURNAL OF PHYSICS D: APPLIED PHYSICS
J. Phys. D: Appl. Phys. **38** (2005) 2204–2210 doi:10.1088/0022-3727/38/13/019

Experimental and calculated N(^{4}S) temporal density profile in the N_2 flowing post-discharge

J Levaton[1], J Amorim[1] and D Franco[2]

[1] Departamento de Física, Instituto Tecnológico de Aeronáutica, Centro Técnico Aeroespacial, 12228-900, São José dos Campos, Brazil
[2] Departamento de Engenharia Ambiental, Universidade Federal de Santa Catarina, 88040-970, PO Box 5039, Florianópolis, Brazil

E-mail: jacques.levaton@ig.com.br and jayr@ita.br

Received 15 March 2005, in final form 18 April 2005
Published 17 June 2005
Online at stacks.iop.org/JPhysD/38/2204

Abstract
The post-discharge generated by a direct current N_2 flowing discharge was studied by optical emission spectroscopy. The experimental conditions were such that the short-lived afterglow could be detected. The post-glow emissions, first positive and 1st negative N_2 systems, were recorded along the post-discharge tube up to times of the order of 0.1 s (late afterglow). The experimental parameters, gas and $N_2(X\,^1\Sigma_g^+)$ vibrational temperatures, were measured and utilized in a numerical kinetic model developed for calculations of the N(^{4}S) absolute density along the post-discharge. Moreover, the model was employed in estimations of the percentage of each excitation channel to the excitation of the $N_2(B\,^3\Pi_g, v = 11)$ state as a function of post-discharge time. Among them, the main excitation channels are the N(^{4}S) three-body recombination and the $N_2(A\,^3\Sigma_u^+)$ pooling with the $N_2(X\,^1\Sigma_g^+, v)$ states. From the computation of the percentage of contribution of the three-body recombination mechanism in the overall excitation of the $N_2(B\,^3\Pi_g, v = 11)$ state, the first positive emission intensity at 580.4 nm wavelength was corrected. After correction, one expects that the emission intensity would be proportional to the square root of the N(^{4}S) density. Therefore, [N(^{4}S)] experimental estimations can be achieved as a function of post-discharge position or post-discharge time. The experimental profiles are in good agreement with our previous theoretical results and the spatial parametrization to the 580.4 nm band provides a significant advance to the experimental method developed by Bockel *et al* (1995 *Surf. Coat. Technol.* **74–75** 474).

1. Introduction

The N_2 post-discharge generated by a pure N_2 flowing discharge is characterized as a function of the residence time since the kinetic mechanisms and glow features change with this last parameter. The post-discharge is usually divided into three regimes [1]: (i) near afterglow ($\tau \sim 10^{-4}$–10^{-2} s), (ii) late or Lewis–Rayleigh afterglow ($\tau \sim 0.1$ s) [2] and the (iii) special regime known as short-lived or pink afterglow [3–6]. The last one is detected only in determined conditions of discharge pressure, power and flow rate. The first positive spectrum is present in any of these regimes. In the near and short-lived afterglows (SLAs) the spectrum in the 570.0–610.0 nm wavelength region presents band head peaks with great intensity for the sequence of transitions with $\Delta v = 4$, that is, $N_2(B\,^3\Pi_g, 6 \leqslant v \leqslant 12)$–$N_2(A\,^3\Sigma_u^+, 2 \leqslant v \leqslant 8)$ [7]. Either in the near or SLA the $N_2(B\,^3\Pi_g, v)$ excitation can be described as the summation of three main

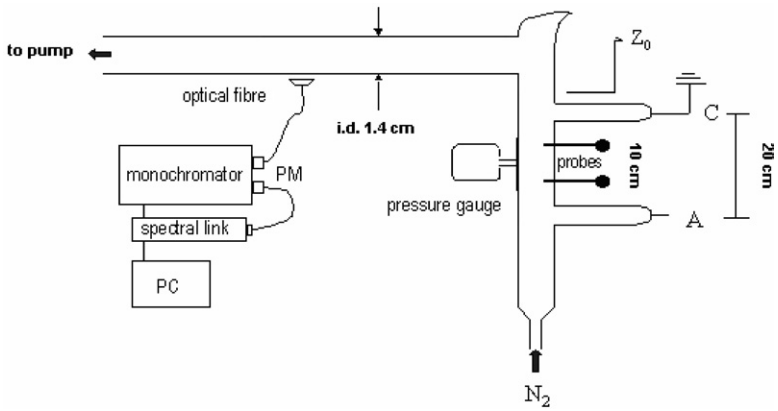

Figure 1. Experimental set-up.

mechanisms [8–10]:

$$N_2(A\,^3\Sigma_u^+, v' = 0, 1) + N_2(A\,^3\Sigma_u^+, v' = 0, 1) \rightarrow N_2(B\,^3\Pi_g, 0 \leqslant v \leqslant 12) + N_2(X\,^1\Sigma_g^+, w), \quad (1)$$

$$N_2(A\,^3\Sigma_u^+, v = 0, 1) + N_2(X\,^1\Sigma_g^+, 4 \leqslant v < 14) \rightarrow N_2(B\,^3\Pi_g, 0 \leqslant v \leqslant 12) + N_2(X\,^1\Sigma_g^+, w), \quad (2)$$

$$N(^4S) + N(^4S) + N_2(X\,^1\Sigma_g^+) \rightarrow N_2(B\,^3\Pi_g, v = 11) + N_2(X\,^1\Sigma_g^+). \quad (3)$$

However, in the SLA a fourth mechanism should be considered in the excitation of the $N_2(B\,^3\Pi_g)$ state. It arises from the quenching of the $N_2(a'\,^1\Sigma_u^-)$ state [11] that reaches significant concentrations. In the Lewis–Rayleigh afterglow ($\tau \sim 0.1$ s) the three-body recombination mechanism [12–19] dominates and the spectrum pattern presents dominance of the band head peak for the transition $N_2(B\,^3\Pi_g, v = 11 \rightarrow A\,^3\Sigma_u^+, v = 7)$.

In order to reflect on the kinetic mechanisms which are related to the generation of the $N_2(B\,^3\Pi_g, v = 11)$ state, one must pay attention to the pressure parameter. Quenching of $N_2(B\,^3\Pi_g, v = 11)$ by N_2 must also be considered, where $k_Q = (2.8 \pm 0.2) \times 10^{-11}$ cm^3 s^{-1} [20]. In the situation where the $N_2(B\,^3\Pi_g, v = 11)$ radiative state is predominantly generated by the three-body recombination mechanism, an estimation for the N(^{4}S) density can be achieved. The degree of accuracy in this estimation depends on knowledge of the percentage of contribution of each mechanism mentioned above (reactions (1)–(3)). Bockel *et al* [21] have developed an experimental method based only on spectroscopic measurements in order to determine the N(^{4}S) relative density profile in the N_2 post-discharge. They have shifted the optical fibre along the post-discharge until a position where the transition intensity at 580.4 nm wavelength presented its maximum with respect to the other transitions concerning the $\Delta v = 4$ sequence (570.0–610.0 nm). At this point, the parametrization factor to $\lambda = 580.4$ nm intensity was considered as 1 (unity). At the beginning of the post-discharge tube, in the near afterglow, under considerations on the N_2 first positive spectrum and the post-discharge kinetics, the authors considered the parametrization factor as 0 (zero). A linear approach was assumed for the intensity parametrization in the positions between these two points.

In this work we employ a numerical model initially developed to describe the N_2 SLA in order to achieve the N(^{4}S) density parametrization factor along the N_2 post-discharge. The parametrization factor is utilized to generate the experimental N(^{4}S) density profile obtained from the first positive system spectroscopic measurements. The experimental N(^{4}S) density spatial profile obtained by Bockel's parametrization is compared with our results. Discrepancies arise in the near afterglow region where our parametrization is substantially different from the one obtained by Bockel.

2. Experiment

The experimental set-up is shown in figure 1. Direct current glow discharges were generated between two electrodes located 20 cm apart, by a power source of 5 KV and current of 150 mA. Two Langmuir probes inserted in the positive column, located 10 cm away from each other between the side-armed electrodes, were utilized in measurements of the electric field. The discharge and post-discharge tubes (1.4 cm i.d.) were fashioned in Pyrex glass and were connected by a Wood trap arrangement. The post-discharge tube constructed was 1 m long. The pressure was measured by means of a Baratron gauge (MKS 722A) and the limit pressure reached the value of 0.02 Torr (2% of the lowest value of pressure utilized in this work). High-purity N_2 gas (99.999%) was utilized. The N_2 flow was controlled by a flow meter (MKS 247C) and maintained by a mechanical vacuum pump of 25 m^3 h^{-1} (E1M18 Edwards). Emissions were studied by means of a monochromator (Jobin–Yvon, THR-1000) with a grating of 1800 g mm^{-1} connected to a photomultiplier tube (Hamamatsu, R928). An optical fibre was utilized to collect the light from several studied positions. We have defined in this experimental set-up the post-discharge initial position located at 1.5 cm after the cathode in the flow sense. This was done on the basis of model adjustment for emission profiles [22]. In this paper we have analysed a specific experimental condition where the discharge current is 30 mA, the flow rate is 450 sccm and the gas pressure is 5 Torr.

3. Results and discussion

The numerical model provides the parametrization factor employed to correct the 580.4 nm band head intensity along the post-discharge. The correction permits one to generate

Table 1. Additional reactions for the numerical model developed and described in [5].

	Supplementary reactions	k ($cm^3\ s^{-1}$) k ($cm^6\ s^{-1}$) $cm^2\ s^{-1}$	References
R01	$N_2(X\,^1\Sigma_g^+, v > 24) + N(^4S) \rightarrow N_2(A\,^3\Sigma_u^+) + N(^4S)$	5×10^{-14}	[24]
R02	$N_2(A\,^3\Sigma_u^+) + N(^4S) \rightarrow N_2(X\,^1\Sigma_g^+, v = 9) + N(^2P)$	4×10^{-11}	[36]
R03	$N_2(X\,^1\Sigma_g^+, v = 9) + N(^2P) \rightarrow N_2(A\,^3\Sigma_u^+) + N(^4S)$	$0.86 \times 10^{-10} \times (1 - e^{-2062/T})/(1 - e^{-3353/T}) \times e^{-1398/T}$	[37]
R04	$N_2^+(X\,^2\Sigma_g^+) + e \rightarrow 0.143 \times N(^4S) + N(^4S)$ $\rightarrow 0.771 \times N(^2D) + N(^4S)$ $\rightarrow 0.086 \times N(^2P) + N(^4S)$	$1.62 \times 10^{-7} \times (300/Te)^{0.39}$	[37]
R05	$N(^4S) + N(^4S) + N_2(X\,^1\Sigma_g^+)$ $\rightarrow N_2(B\,^3\Pi_g, v = 11) + N_2(X\,^1\Sigma_g^+)$	$8.3 \times 10^{-34} \exp(500/T)$ 1.3×10^{-33}	[37] [38]
R06	$N(^2D) + N_2(X\,^1\Sigma_g^+) \rightarrow N(^4S) + N_2(X\,^1\Sigma_g^+)$	2×10^{-14}	[39]
R07	$N(^2P) + N_2(X\,^1\Sigma_g^+) \rightarrow N(^4S, ^2D) + N_2(X\,^1\Sigma_g^+)$	6×10^{-14}	[39]
R08	$N(^2P) + N(^4S) \rightarrow N(^2D) + N(^4S)$	1.8×10^{-12}	[37]
R09	$N_2(A\,^3\Sigma_g^+) \rightarrow$ diffusion	$0.179 \times (760/p) \times (T/273)^{1.9}$	[40]

the experimental $N(^4S)$ temporal density profile consequent to the contribution of the reactions, but reaction (3) is eliminated. The main body of the numerical model was described elsewhere [4]. We have adapted it to include the important mechanism:

$$N_2(A\,^3\Sigma_u^+) + N(^4S) \rightarrow N_2(X\,^1\Sigma_g^+) + N(^2P), \qquad (4)$$

which was not considered in our last work. Moreover, we have updated the model by including an important mechanism described by Loureiro *et al* [5]. This is the following reaction:

$$N_2(X\,^1\Sigma_g^+, v \geqslant 25) + N(^4S) \rightarrow N_2(A\,^3\Sigma_u^+) + N(^4S). \qquad (5)$$

We have obtained a rough experimental estimation for the rate constant of this reaction as described in [23, 24]. This value lies at $5 \times 10^{-14}\ cm^3\ s^{-1}$. The set of reactions that supplement the main body of the numerical model is described in table 1. Another modification introduced in the model is that it accepts temporal gas temperature profiles as entries in order to vary all the rate constants that are temperature dependent. This includes the set of V–V and V–T exchange reactions, which were taken from [25].

We have included the initial condition for the atomic metastable states $N(^2D)$ and $N(^2P)$: $[N(^2D)] = 5 \times 10^{12}\ cm^{-3}$ and $[N(^2P)] = 1.5 \times 10^{12}\ cm^{-3}$. These values were chosen on the basis of experimental measurements carried out in the Ar–N_2 post-discharge and we have discussed these in a previous work [24].

In figure 2, we present the temporal variation of some experimental densities of excited states along the post-discharge, and in figure 3 we present the gas temperature variation through the post-discharge. The gas temperature was measured by optical emission spectroscopy (OES) employing the first positive system emissions. Hochard *et al* [26] obtained synthetic spectra of the first positive emissions in the range 700–778 nm. From the ratio of the intensities of bands emitted at 774.4 and 773.0 nm the authors calculated the rotational temperature of the $N_2(B\,^3\Pi_u)$ state, which can be used to estimate the gas temperature. It can be verified that the SLA is present since the first negative emissions are observed in the post-discharge spectra (see the full circles profile in figure 2). The analysis of the density profiles indicates that the pink

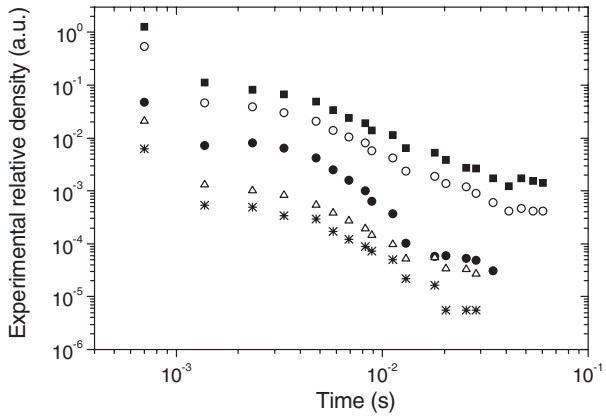

Figure 2. Radiative states relative density profiles. $N_2(B\,^3\Pi_g, v = 6)$ (■), $N_2(B\,^3\Pi_g, v = 9)$ (○), $N_2(C\,^3\Pi_u, v = 0)$ (△), $N_2(C\,^3\Pi_u, v = 4)$ (∗) and $N_2^+(B\,^2\Pi_u, v = 0)$ (●).

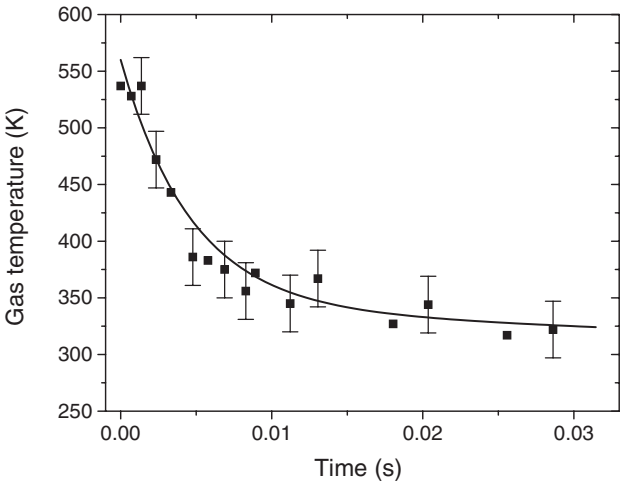

Figure 3. Gas temperature post-discharge profile.

afterglow phenomenon occurrs in a weak form as there are no remarkable peaks in the density profiles, as are usually observed [3, 4]. Following the work of Bockel *et al* [21] we have verified that the first positive spectrum starts to present dominance of the $N_2(B\,^3\Pi_g, v = 11) \rightarrow N_2(A\,^3\Sigma_u^+, v' = 7)$

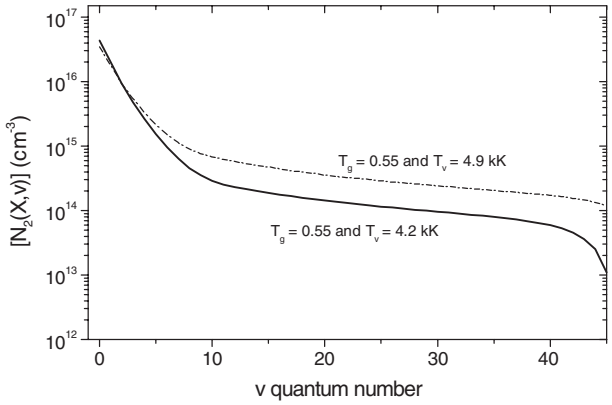

Figure 4. Treanor–Gordiets $N_2(X\,^1\Sigma_g)$ vibrational distributions. The dashed curve was calculated for $T_v = 4.9$ kK and $T_g = 0.55$ kK and the solid curve was calculated for $T_v = 4.2$ kK and $T_g = 0.55$ kK.

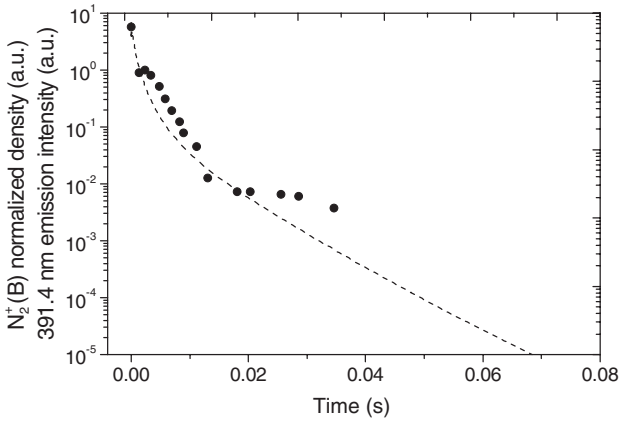

Figure 5. $N_2^+(B\,^2\Pi_u, v = 0)$ relative density. Experimental (●) and calculated (- - - -) values.

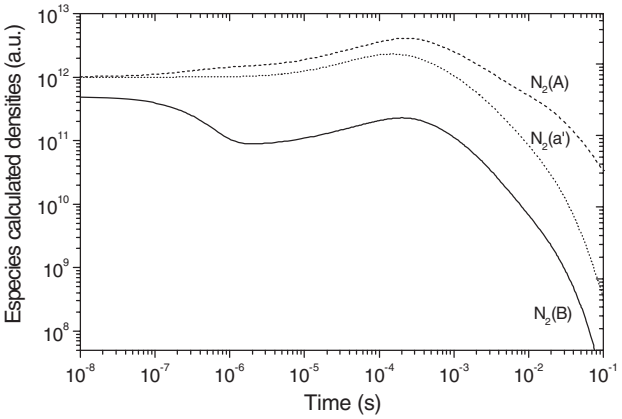

Figure 6. Calculated densities temporal profiles. $N_2(A\,^3\Sigma_u^+)$ (- - - -), $N_2(a'\,^1\Sigma_u^-)$ (· · · · · ·) and $N_2(B\,^3\Pi_g)$ (——).

transition at post-discharge times longer than 9 ms and that this effect is maximum at 41.5 ms. The $N_2(X\,^1\Sigma_g^+)$ vibrational temperature was measured following the method presented in [27], and the electronic density was measured by the double probes technique with the application of the electrons-drift velocity presented by Raizer [28]. It should be mentioned that these measurements were done in the discharge and are inputs to the numerical model. The values found are: 5.0 ± 0.8 kK and 7.4×10^{10} cm^{-3}, respectively. The low vibrational temperature of the discharge should be the explanation for the absence of peaks in the density profiles of the radiative species.

In order to achieve reliable results with the numerical model we have chosen to apply the vibrational temperature value of 4.2 kK. This was done because the initial VDF utilized in this model is the analytical form of the Trenor–Gordiets VDF [29]. It is clear that the analytical form does not account for the N_2–N quenching mechanism which leads one to find overpopulated VDFs with respect to those obtained by self-consistent numerical models [30]. In figure 4 we present the analytical Treanor–Gordiets VDFs calculated for $T_v = 4.9$ and 4.2 kK and $T_g = 0.55$ kK. For the lower vibrational temperature the VDF presents the expected plateau and tail decay as those ones obtained by Loureiro *et al* [5] with a N_2 discharge self-consistent model. The analytical Treanor–Gordiets distribution obtained for $T_v = 4.2$ kK and $T_g = 0.55$ kK could be approximated to a VDF calculated by Loureiro with $T_v = 4.0$ kK and $T_g = 0.40$ kK. The numerical model results are presented in figures 5 and 6. In figure 5 we have presented the 391.4 nm normalized emission intensity that represents the $N_2^+(B\,^2\Pi_u, v = 0)$ state and the corresponding calculated density profile. Both curves were normalized at $t = 0$. Despite the little peak which appears in the experimental profile, the model fits the ionic profile relatively well. The calculated molecular metastable densities, $N_2(A\,^3\Sigma_u^+)$ and $N_2(a'\,^1\Sigma_u^-)$ and the $N_2(B\,^3\Pi_g)$ calculated density are plotted in figure 6. The model was not elaborated in order to separate the vibrational levels of each electronic excited state in the case of density profiles generation. The increase in the metastables density shown in the density profiles from 10^{-4} s is a result of the increase in the global excitation due to the vibrational relaxation. The important reactions responsible for the $N_2(A\,^3\Sigma_u^+)$ metastable density increase are the reactions R01 and R03 presented in table 1.

We have employed the numerical model in order to analyse the contribution of the main reactions to the $N_2(B\,^3\Pi_g, v = 11)$ excitation. They are the reactions (1)–(3) described in the introductory section and the following reaction:

$$N_2(a'\,^1\Sigma_u^-) + N_2(X\,^1\Sigma_g^+) \rightarrow N_2(B\,^3\Pi_g) + N_2(X\,^1\Sigma_g^+), \quad (6)$$

whose rate-constant was measured by Piper [11] as being 1.9×10^{-13} cm^3 s^{-1}. We have estimated the branching ratio of reactions (2) and (6) by applying the Franck–Condon factors to each vibrational level involved in the excitation of the $N_2(B\,^3\Pi_g, v)$ levels. We have considered the excitation occurring from the $N_2(X\,^1\Sigma_g^+, v)$ as suggested by Piper [9]. In reactions (1) and (2) we have considered the first two vibrational levels of the $N_2(A\,^3\Sigma_u^+)$ state to be in agreement with the branching ratios presented by Piper for reaction (1). Therefore, the model requires the ratio $N_2(A\,^3\Sigma_u^+, v = 1)/N_2(A\,^3\Sigma_u^+, v = 0)$ as input. This information was obtained from Cernogora [31] and from the works of Rajesh and Ghosh [32]. They have described N_2 discharges with characteristics similar to the discharge studied in this work. We are employing the value 1.3 in the ratio between the first two vibrational populations of the $A\,^3\Sigma_u^+$ state. In reaction (6) we consider only the fundamental vibrational level of the $a'\,^1\Sigma_u^-$ state. The branching rate constants for the specific $N_2(B\,^3\Pi_g, v = 11)$ excitation are presented in table 2. We should stress that these constants were employed exclusively in the computation of the

Table 2. Specific reactions accounting for the $B\,^3\Pi_g$, $v = 11$ excitation.

	$B\,^3\Pi_g$, $v = 11$ excitation reactions	k (cm^3 s^{-1})
B01	$N_2(A\,^3\Sigma_u^+, v = 0) + N_2(X\,^1\Sigma_g^+, v = 13) \rightarrow N_2(B\,^3\Pi_g, v = 11) + N_2(X\,^1\Sigma_g^+)$	2.7×10^{-13}
B02	$N_2(A\,^3\Sigma_u^+, v = 1) + N_2(X\,^1\Sigma_g^+, v = 12) \rightarrow N_2(B\,^3\Pi_g, v = 11) + N_2(X\,^1\Sigma_g^+)$	1.5×10^{-12}
B03	$N_2(a'\,^1\Sigma_u^-, v = 0) + N_2(X\,^1\Sigma_g^+, v = 4) \rightarrow N_2(B\,^3\Pi_g, v = 11) + N_2(X\,^1\Sigma_g^+)$	3.5×10^{-16}
B04	$N_2(A\,^3\Sigma_u^+, v = 0) + N_2(A\,^3\Sigma_u^+, v = 0) \rightarrow N_2(B\,^3\Pi_g, v = 11) + N_2(X\,^1\Sigma_g^+)$	3.2×10^{-12}
B05	$N_2(A\,^3\Sigma_u^+, v = 0) + N_2(A\,^3\Sigma_u^+, v = 1) \rightarrow N_2(B\,^3\Pi_g, v = 11) + N_2(X\,^1\Sigma_g^+)$	4.0×10^{-12}
B06	$N_2(A\,^3\Sigma_u^+, v = 1) + N_2(A\,^3\Sigma_u^+, v = 1) \rightarrow N_2(B\,^3\Pi_g, v = 11) + N_2(X\,^1\Sigma_g^+)$	1.0×10^{-11}

Reactions rate constant from [9, 11, 20].

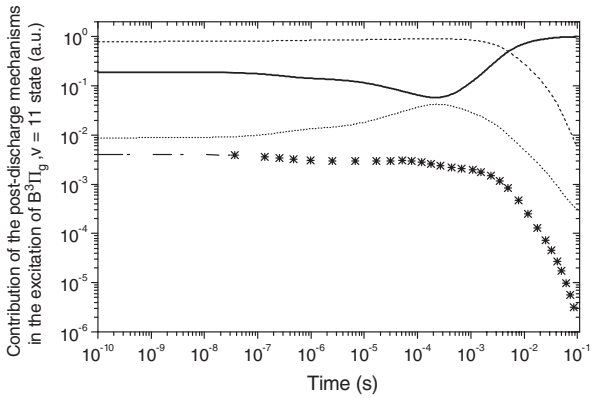

Figure 7. Percentage of contribution of each mechanism to the $N_2(B\,^3\Pi_g, v = 11)$ excitation. Reaction (R05—table 1) (——), reactions (B01 and B02—table 2) (- - - -), reactions (B04–B06) (· · · · · ·) and reaction (B03) (∗).

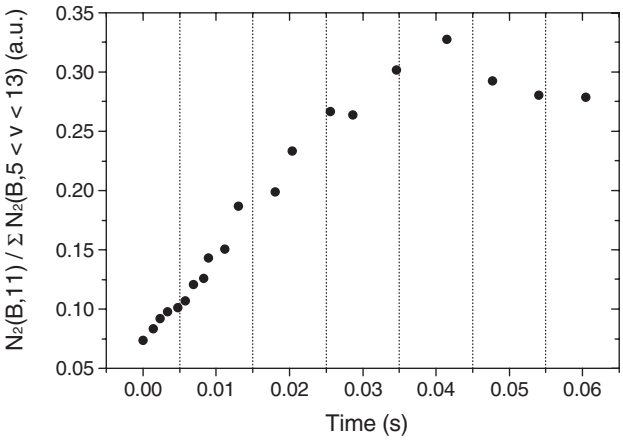

Figure 8. Normalized values of the $N_2(B\,^3\Pi_g, v = 11)$ density.

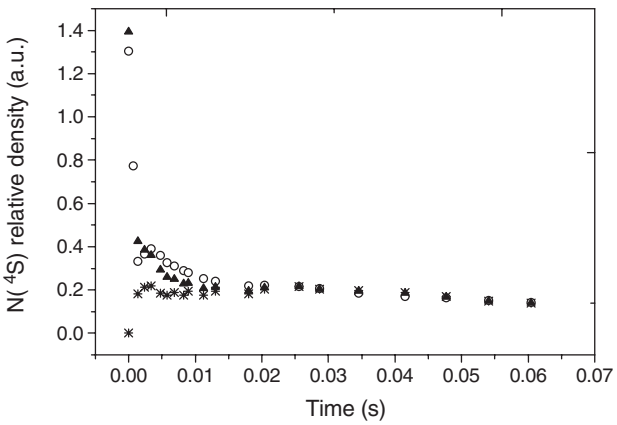

Figure 9. N(^{4}S) temporal density profiles. The density profile generated by Bockel's parametrization, equations (8) and (9), is represented by the star symbols. The density profile obtained from the numerically generated boundary conditions (equations (10) and (11)) is represented by the triangle symbols. The density profile obtained completely by the numerically generated correction factor (figure 7) is represented by the circle symbols. See table 3 with the summary of conditions.

$N_2(B\,^3\Pi_g, v = 11)$ excitation while the density profiles were calculated with the total rate constants. Moreover, in the last case, only the fundamental vibrational states were considered.

Figure 7 presents the contribution of reactions described in table 2 and reaction R05 (table 1) to the excitation of the $N_2(B\,^3\Pi_g, v = 11)$ state. The solid curve represents the reaction R05 with the constant depending on the gas temperature parameter (see figure 3). We have obtained values for the 580.4 nm intensity parametrization that differ from those proposed by Bockel. In the early afterglow ($\sim 10^{-4}$ s) the correction factor is 0.06 instead of 0 (zero). In the late afterglow (0.1 s) the correction factor is 0.98 instead of 1 (unity). In fact, we have chosen the initial value of parametrization as 0.19, taken at $t \sim 10^{-7}$ s that is the typical time for the EEDF relaxation in the post-discharge. The employment of the correction factor as 0.06 generates a stronger density gradient in the N_2 post-discharge. However, we have verified that the density profile general features are unchanged. The N(^{4}S) density is furnished by the equation:

$$[\mathrm{N}(^4\mathrm{S})](t) \propto \sqrt{\frac{I_{580.4}(t)C(t)(\nu_{\mathrm{rad}} + k_{\mathrm{Q}}[\mathrm{N_2}](t))}{[\mathrm{N_2}](t)}}, \qquad (7)$$

where $C(t)$ is the parametrization factor and k_{Q} is the $N_2(B\,^3\Pi_g, v = 11)$ quenching rate constant (see introductory section). The N_2 density is a function of the gas temperature variation with time.

As discussed in the introduction, Bockel's parametrization follows from the ratio between the $N_2(B\,^3\Pi_g, v' = 11)$ and the summation of the $N_2(B\,^3\Pi_g, 6 \leqslant v \leqslant 12)$ densities. Our relative density experimental values are presented in figure 8.

The N(^{4}S) density profiles as a function of time are shown in figure 9 for conditions presented in table 3. The star symbols profile was calculated following Bockel's parametrization. For that we have employed the values presented in figure 8 scaled following the boundary conditions:

$$C(t = 0) = 0 \qquad (8)$$

and

$$C(t = t_{\mathrm{max}} = 41.5\,\mathrm{ms}) = 1. \qquad (9)$$

Table 3. Summary of calculated and experimental data employed in the N(^{4}S) density profile measurements.

Model input parameters: $T_v\{N_2(X\ ^1\Sigma_g^+)\} = 5.0 \pm 0.8$ kK (E)[a], T_g (see figure 3) (E), $n_e = 7.4 \times 10^{10}$ cm^{-3} (E), $[N_2(A\ ^3\Sigma_u^+, v = 0)]/[N_2(A\ ^3\Sigma_u^+, v = 1)] = 1.3$ (E) and (C)[a] [31,32].			
Post-discharge boundary conditions (bc) and parametrization factor	This work. Bockel's profile (figure 9—star symbols). Experimental parametrization from the $N_2(B\ ^3\Pi_g)$ normalized VDF (figure 8)	This work. Experimental parametrization from the $N_2(B\ ^3\Pi_g)$ normalized VDF scaled by the model bc. (figure 9, triangles)	This work. Calculated parametrization from the post-discharge model and (figure 7, solid line figure 9, circle symbols)
t_i (ms) and t_f (ms)	0 and 41.5 ms	0 and 41.5 ms	0–100 ms
$C(t)$[b]	0 and 1	0.19 and 0.98	Solid line in figure 7

[a] (E) Experimental data and (C) Calculated data. [b] $C(t)$ is the parametrization factor at the instant t.

The triangle symbols profile was calculated following the results obtained with our model and discussed previously (see figure 7). In this case, the values presented in figure 8 are differently scaled, following model-generated boundary conditions:

$$C(t = 0) = 0.19 \tag{10}$$

and

$$C(t = t_{max}) = 0.98. \tag{11}$$

The circle symbols profile follows a different parametrization where $C(t)$ is completely obtained by numerical results (solid line in figure 7). The N(^{4}S) density profile in this situation presents a peak at $t \sim 4$ ms, which is close to the time of maximum intensity measured for the excited ion in the pink afterglow ($t \sim 2.5$ ms). The reader should refer to figure 5 to verify the slight increase in the excited-ion density. This behaviour for the N(^{4}S) atoms was observed in the N_2 pink afterglow of a microwave discharge by the mass spectrometry technique [33]. The possible kinetic mechanisms to explain it are discussed in [4,5]. The other N(^{4}S) profile obtained by our numerical results parametrization (triangles) can be compared with that obtained by Bockel's parametrization. It seems that our model provides more realistic parameters for the end of discharge and the late afterglow since the temperature gradient (see figure 3) seems to be insufficient to explain the increase in the N(^{4}S) density obtained by Bockel's parametrization. Mazouffre *et al* [34] have measured the N(^{4}S) absolute density profile by two-photon absorption laser-induced fluorescence (TALIF, [35]) in the SLA of a microwave discharge at 440 Pa (3.3 Torr). Its behaviour is very similar to the one obtained here when we apply the boundary conditions utilized by Bockel *et al* [21] (figure 9, star symbols). However, the molecular gas temperature decreases from 1 to 0.3 kK, from the end of the discharge to the downstream part of the SLA. The N(^{4}S) atoms temperature presents a gradient of 1.4–0.3 kK in the same post-discharge region. In Mazouffre *et al*'s work [34], two important factors can be assigned to the absence of a remarkably high N(^{4}S) density peak in the highly excited SLA as Morrits [33] has observed and we have measured: the absolute pressure value, which is low with respect to those studied in the Morrits thesis and the very strong gas temperature gradient with respect to the ones obtained in a dc discharge. Our previous calculations [4] have shown that the N(^{4}S) density increases can happen locally in the SLA as pressure increases. The correction parameter to the 580.4 nm emission intensity was studied as a function of the three-body excitation reaction rate constant (reaction R05). The correction

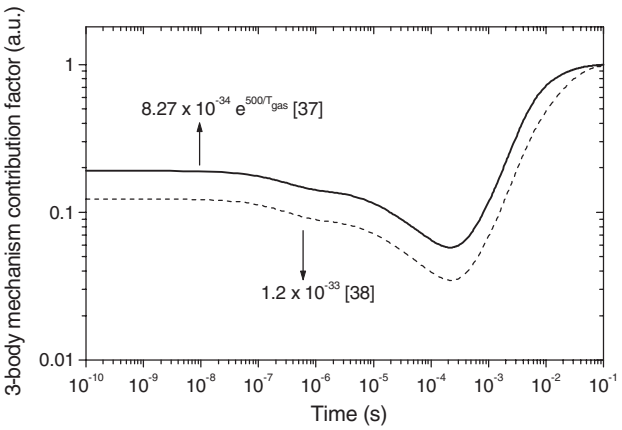

Figure 10. Comparison of correction factors for different rate constants of reaction R05 in table 1.

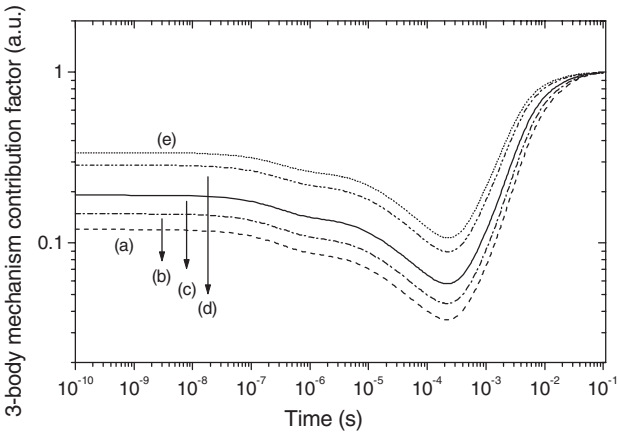

Figure 11. Comparison of correction factors for some ratios $N_2(A\ ^3\Sigma_u^+, v = 1)/N_2(A\ ^3\Sigma_u^+, v = 0)$. (a) 0.1, (b) 0.5, (c) 1.3, (d) 5 and (e) 11.

parameter profiles are presented in figure 10. Density profiles can change appreciably with this rate constant. In this work, we have chosen to consider the effects of the measured gas-temperature profile in the study. In figure 11 we present the result of an analysis concerning the effects of the vibrational distribution of the $N_2(A\ ^3\Sigma_u^+)$ state in the correction factor. The analysed ratios $N_2(A\ ^3\Sigma_u^+, v = 1)/N_2(A\ ^3\Sigma_u^+, v = 0)$ are: (a) 0.1, (b) 0.5, (c) 1.3, (d) 5 and (e) 11. It is clear that the resultant atomic density profile depends strongly on the $A\ ^3\Sigma_u^+$ vibrational distribution. This behaviour results from

the Franck–Condon approximation utilized in the branching ratios determination. We have chosen the ratio corresponding to an experimental vibrational distribution measured by Cernogora [31] in experimental conditions very similar to ours. Moreover, this vibrational distribution was compared with the numerical results of Rajesh and Gosh [32] N_2 discharge model whose simulating parameters (p, n_e, R) are very similar to ours.

4. Conclusions

In this paper we have proposed the improvement of an OES method to analyse the first positive spectrum emissions in order to obtain estimations of the N(^{4}S) density in the N_2 post-discharge. This method is based on theoretical data obtained from a numerical model developed to simulate the N_2 SLA. We have obtained three different N(^{4}S) density profiles depending on the parametrization factors (figure 9). The first one was obtained by replication of Bockel's work [21]. The other two were obtained through our numerical results. In one case we have employed the parametrization factors scaled for the following boundary conditions (10) and (11) to the N(^{4}S) signal described by equation (7). In the second case we have employed the complete profile of the percentage of contribution of the three-body recombination mechanism in the $N_2(B\,^3\Pi_g, v = 11)$ to correct the N(^{4}S) signal. The last choice has produced a temporal N(^{4}S) profile with a maximum at $t \sim 4$ ms, which is in accordance with some published experimental and theoretical results. Morrits [33] has obtained the N(^{4}S) density profiles by the mass spectrometry technique. We can conclude that the method proposed by Bockel *et al* [21] was improved in this work with the application of the numerical model.

Acknowledgments

J Levaton is grateful for extremely helpful discussions with Dr L N G Rosh and Dr I N Marino and he is indebted to Dr S G Trees and Dr B O Israel for discussions concerning the modelling and the text.

References

[1] Ricard A and Souza A R 1994 *J.Physique III (France)* **4** 2593
[2] Wright A N and Winkler C A 1968 *Active Nitrogen* (London: Academic)
[3] Supiot P, Dessaux O and Goudmand P 1995 *J. Phys. D: Appl. Phys.* **28** 1826
[4] Levaton J, Amorim J, Souza A R, Franco D and Ricard A 2002 *J. Phys. D: Appl. Phys.* **35** 689
[5] Loureiro J, Sá P A and Guerra V 2001 *J. Phys. D: Appl. Phys.* **34** 1769
[6] Guerra V, Sá P A and Loureiro J 2002 *Phys. Rev.* E **63** 046404-1
[7] Lofthus A and Krupenie P H 1977 *J. Phys. Chem. Ref. Data* **6** 113
[8] Nadler I and Rosenwaks S 1985 *J. Chem. Phys.* **83** 3932
[9] Piper L G 1989 *J. Chem. Phys.* **91** 864
[10] Amorim J, Baravian G and Ricard A 1995 *Plasma Chem. Plasma Proc.* **15** 721
[11] Piper L G 1989 *J. Chem. Phys.* **87** 1625
[12] Lewis E P 1900 *Ann. Phys., Lpz.* **2** 459
[13] Lewis E P 1900 *Astrophys. J.* **12** 8
[14] Lewis E P 1904 *Phys. Rev.* **18** 125
[15] Strutt R J 1911 *Proc. R. Soc.* A **85** 219
[16] Strutt R J and Fowler A 1912 *Proc. R. Soc.* A **86** 105
[17] Strutt R J 1912 *Proc. R. Soc.* A **86** 56
[18] Strutt R J 1913 *Proc. R. Soc.* A **88** 539
[19] Rabinowitch 1937 *Trans. Faraday Soc.* **33** 283
[20] Piper L G 1988 *J. Chem. Phys.* **88** 6911
[21] Bockel S, Diamy A M and Ricard A 1995 *Surf. Coat. Technol.* **74–75** 474
[22] Levaton J 2004 *PhD Thesis* Universidade Federal de Santa Catarina, Florianópolis, Brazil
[23] Levaton J, Monna V, Amorim J and Ricard A 2003 *Proc. 13th CIP (Antibes, France, 2003)*
[24] Levaton J, Kiohara V and Amorim J 2003 *Proc. 16th ISPC (Taormina, Italy, 2003)* contribution no 271
[25] Loureiro J and Ferreira C M 1986 *J. Phys. D: Appl. Phys.* **19** 17
[26] Hochard L, Magne L, Cernogora G and Peeters J 1994 *Proc. 12th European Sectional Conf. on the Atomic and Molecular Physics of Ionized Gases (Noordwijkerhout, The Netherlands, 1994)* vol 18E, p 336
[27] Levaton J, Amorim J, Monna V, Nagai J and Ricard A 2004 *Eur. Phys. J. Appl. Phys.* **26** 59
[28] Raizer Y P 1991 *Gas Discharge Physics* (Berlin: Springer)
[29] Gordiets B F, Hamedov S S and Shelepin L A 1975 *Sov. Phys.—JETP* **40** 640
[30] Loureiro J 1991 *Chem. Phys.* **157** 157
[31] Cernogora G 1981 *PhD Thesis* Université Paris-XI, Orsay, France
[32] Rajesh N and Ghosh P K 1990 *J. Phys. D: Appl. Phys.* **23** 1663
[33] Morrits A 1997 *PhD Thesis* Université Paris-XI, Orsay, France
[34] Mazouffre S, Foissac C, Supiot P, Vankan P, Engeln R, Schram D C and Sadeghi N 2001 *Plasma Sources Sci. Technol.* **10** 168
[35] Amorim J, Baravian G and Jolly J 2000 *J. Phys. D: Appl. Phys.* **33** R51
[36] Piper L G 1989 *J. Chem. Phys.* **90** 12 7087
[37] Matveyev A A and Silakov V P 1999 *Plasmas Sources Sci. Technol.* **8** 162
[38] Ung A Y M 1976 *J. Chem. Phys.* **65** 2987
[39] Lin C L and Kaufman F 1971 *J. Chem. Phys.* **55** 3760
[40] Capitelli M, Ferreira C M, Gordiets B F and Osipov A I 2000 *Plasmas Kinetics in Atmospheric Gases* (Berlin: Springer)